TPC1 deficiency or blockade augments systemic anaphylaxis and mast cell activity

Elisabeth Arlt[a], Marco Fraticelli[a], Volodymyr Tsvilovskyy[b], Wiebke Nadolni[a], Andreas Breit[a], Thomas J. O'Neill[a], Stefanie Resenberger[a], Gunther Wennemuth[c], Christian Wahl-Schott[d], Martin Biel[e], Christian Grimm[a], Marc Freichel[b], Thomas Gudermann[a], Norbert Klugbauer[f], Ingrid Boekhoff[a,1,2], and Susanna Zierler[a,1,2]

[a]Walther Straub Institute of Pharmacology and Toxicology, Ludwig-Maximilians-Universität München, 80336 München, Germany; [b]Institute of Pharmacology, University of Heidelberg, 69120 Heidelberg, Germany; [c]Institute for Anatomy, University of Duisburg-Essen, 45147 Duisburg, Germany; [d]Institute for Neurophysiology, Hannover Medical School, 30625 Hannover, Germany; [e]Department of Pharmacy, Ludwig-Maximilians-Universität München, 81377 München, Germany; and [f]Institute for Experimental and Clinical Pharmacology and Toxicology, Medical Faculty, Albert-Ludwigs-Universität, 79104 Freiburg, Germany

Edited by Michael D. Cahalan, University of California, Irvine, CA, and approved June 5, 2020 (received for review November 15, 2019)

Mast cells and basophils are main drivers of allergic reactions and anaphylaxis, for which prevalence is rapidly increasing. Activation of these cells leads to a tightly controlled release of inflammatory mediators stored in secretory granules. The release of these granules is dependent on intracellular calcium (Ca^{2+}) signals. Ca^{2+} release from endolysosomal compartments is mediated via intracellular cation channels, such as two-pore channel (TPC) proteins. Here, we uncover a mechanism for how TPC1 regulates Ca^{2+} homeostasis and exocytosis in mast cells in vivo and ex vivo. Notably, in vivo TPC1 deficiency in mice leads to enhanced passive systemic anaphylaxis, reflected by increased drop in body temperature, most likely due to accelerated histamine-induced vasodilation. Ex vivo, mast cell-mediated histamine release and degranulation was augmented upon TPC1 inhibition, although mast cell numbers and size were diminished. Our results indicate an essential role of TPC1 in endolysosomal Ca^{2+} uptake and filling of endoplasmic reticulum Ca^{2+} stores, thereby regulating exocytosis in mast cells. Thus, pharmacological modulation of TPC1 might blaze a trail to develop new drugs against mast cell-related diseases, including allergic hypersensitivity.

anaphylaxis | two-pore channel | calcium | mast cell degranulation | histamine

The prevalence for allergies is dramatically increasing worldwide. In severe cases, anaphylaxis, an acute, life-threatening systemic hypersensitivity reaction to food, drugs, or insect stings, may develop. Anaphylaxis is mediated by immunoglobulin (Ig) E-dependent activation of basophils and mast cells (1–3). Mast cells are essential effectors in allergic reactions and are classically activated via cross-linking of IgE receptors ($F_c\varepsilon RI$) upon binding of a specific allergen to precoupled IgE antibodies (4). Upon stimulation, mast cells release preformed mediators from lysosome-related secretory granules, followed by new mediator synthesis and secretion. These mediators include histamine, proteases, cytokines, and growth factors (5, 6). Mast cells are essentially present in all organs, especially in close proximity to blood vessels, neurons, and lymphatic vessels, enabling them to disseminate local inflammatory signals (7). Aside from IgE antibodies, mast cell activation can be triggered by many other stimuli, including Toll-Like Receptor (TLR) ligands, complement-derived peptides, and neuropeptides (7). Depending on the stimulus, diverse patterns of Ca^{2+} mobilization and oscillation emerge, triggering distinct mast cell signaling pathways (8–10).

It is well established that components of the store-operated Ca^{2+} entry pathway promote mast cell activation in vitro and in vivo (11–13). However, although extracellular Ca^{2+} influx enhances exocytosis, intracellular Ca^{2+} release is sufficient for mast cell degranulation (8). To date, our current understanding as to how different spatial and temporal intracellular Ca^{2+} signals are integrated is still very limited. Nonetheless, a complex interplay of all organelles involved in both release and uptake of Ca^{2+} is assumed to maintain cellular Ca^{2+} homeostasis (14, 15). This Ca^{2+} signaling network encompasses the classical intracellular Ca^{2+} store organelle, the endoplasmic reticulum (ER), but also the Golgi apparatus, mitochondria and endolysosomal compartments, all of which are contemplated to closely interact to maintain and facilitate intracellular Ca^{2+} signals. The ER inositol-tri(s)-phosphate (IP_3) receptor (IP_3R) has been suggested to be involved in Ca^{2+} refilling of lysosomes (15, 16). Vice versa, mobilization of lysosomal Ca^{2+} stores was shown to be sufficient to evoke ER-dependent Ca^{2+} release via the IP_3R (17). Regarding the underlying molecular mechanism, endolysosome–ER membrane contact sites have been proposed with the endolysosomal two-pore channel (TPC) proteins localizing to and triggering the formation of these contacts (18). TPCs have further been proposed as targets for nicotinic acid adenine dinucleotide phosphate (NAADP) (19–21), and $PI(3,5)P_2$ has been suggested as crucial for channel activity (22–24). TPCs form a

Significance

The worldwide prevalence of allergic and anaphylactic reactions has increased massively over recent decades. Mast cells and basophils are essential drivers of these diseases, releasing inflammatory mediators such as histamine. Here, we link the endolysosomal two-pore channel TPC1 to systemic anaphylaxis in vivo and underlying mast cell function ex vivo. TPC1-deficient mice develop enhanced systemic anaphylaxis reflected by a drop in body temperature and slower recovery compared to wild-type animals. Genetic deletion or pharmacological inhibition of TPC1 enhances mast cell degranulation and histamine release due to accelerated calcium release, mainly from the endoplasmic reticulum. Accordingly, it is tempting to speculate that activation of TPC1 ameliorates mast cell degranulation, highlighting TPC1 as a potential drug target against allergic hypersensitivity.

Author contributions: I.B. and S.Z. designed research; E.A., M. Fraticelli, V.T., W.N., A.B., T.J.O., S.R., G.W., and S.Z. performed research; C.W.-S., M.B., C.G., and N.K. contributed new reagents/analytic tools; E.A., M. Fraticelli, V.T., W.N., A.B., G.W., M. Freichel, T.G., I.B., and S.Z. analyzed data; and E.A., T.G., I.B., and S.Z. wrote the paper.

The authors declare no competing interest.

This article is a PNAS Direct Submission.

[1]I.B. and S.Z. contributed equally to this work.

[2]To whom correspondence may be addressed. Email: ingrid.boekhoff@lrz.uni-muenchen.de or susanna.zierler@lrz.uni-muenchen.de.

This article contains supporting information online at https://www.pnas.org/lookup/suppl/doi:10.1073/pnas.1920122117/-/DCSupplemental.

First published July 13, 2020.

novel class of nonselective cation channels located in the endolysosomal system with two functional members in the mammalian genome (TPC1 and TPC2) (19, 22, 24). TPCs are thought to participate in the regulation of multiple endolysosomal trafficking pathways and are implicated in various pathological settings, such as lysosomal storage (25) and metabolic (26) or infectious diseases (27). TPCs are thought to control Ca^{2+} signaling in secretory lysosomes, that is, lytic granules of isolated human $CD8^+$ T lymphocytes, thereby ensuring accurate exocytosis in this type of immune cell (28). However, their role in other immune cells containing lysosome-related organelles, such as mast cells (29), remains elusive.

Here, we propose a mechanism for how TPC1 controls intracellular Ca^{2+} homeostasis between the ER and endolysosomal organelles. Importantly, we demonstrate a crucial impact of TPC1 deletion on mast cell-mediated immune responses. Utilizing a TPC1-deficient mouse model, we define an essential role of TPC1 for allergic reactions in a model of systemic anaphylaxis in vivo and decipher underlying defects in the degranulation of basophils and mast cells ex vivo, highlighting TPC1 as a potential target for the treatment of allergic reactions, anaphylaxis and other mast cell-related diseases.

Results

TPC1 Deficiency Results in Enhanced Anaphylaxis due to Increased Inflammatory Mediator Release. TPCs have been implicated in viral infection, immune cell reactivity, and exocytosis of lytic granules of $CD8^+$ T lymphocytes (27, 28, 30). For allergic reactions, exocytosis of histamine and other inflammatory mediators is central. Therefore, we wondered whether TPC1-deficient ($Tpc1^{-/-}$) mice (31, 32) showed altered allergic reactions in a model of passive systemic anaphylaxis (33). To induce systemic anaphylaxis in wild-type ($Tpc1^{+/+}$) and TPC1-deficient ($Tpc1^{-/-}$) mice, animals were sensitized with anti-Dinitrophenyl (DNP) IgE, and, 24 h later, a passive systemic anaphylactic reaction was induced by intravenous (i.v.) application of a solution containing DNP-bovine serum albumin (BSA), thereby inducing mast cell histamine release while circumventing a contribution of the adaptive immune system to the observed phenotype.

An expected immediate drop in the body temperature, credibly due to histamine-induced vasodilatation, was observed with its maximum at about 30 min in $Tpc1^{+/+}$ and at about 40 min after application of the antigen in $Tpc1^{-/-}$ mice. Within 2 h, the body temperature nearly completely recovered to baseline values in $Tpc1^{+/+}$ mice (Fig. 1*A*). Body temperature levels dropped to significantly lower bottom levels in TPC1-deficient animals and were about 1 °C lower (Fig. 1*A*) compared to $Tpc1^{+/+}$ mice. Most strikingly, recovery of the body temperature was significantly delayed in $Tpc1^{-/-}$ compared to $Tpc1^{+/+}$ animals, indicating that the systemic anaphylactic response was significantly accelerated upon TPC1 depletion.

As mast cells are a main source of histamine, we next asked whether mast cell numbers or reactivity were increased in TPC1-deficient animals. Global deletion of TPC1 was verified in primary murine $Tpc1^{-/-}$ cells, isolated via peritoneal lavage (Fig. 1*B*) as well as from bone marrow (*SI Appendix*, Fig. S1*A*). To assess a potential effect of TPC1 deletion on the formation of different immune cell types, we analyzed the proportion of lymphocytes, macrophages, neutrophils, and mast cells present in the peritoneal cavity using flow cytometric analysis. We did not observe differences in the prevalence of T lymphocytes, B lymphocytes, or neutrophils between the two genotypes (Table 1). However, macrophages and mast cells were underrepresented in the peritoneum of $Tpc1^{-/-}$ mice. Among the peritoneal cells obtained from $Tpc1^{+/+}$ mice, macrophages accounted for ∼41%, while, in $Tpc1^{-/-}$ derived peritoneal cells, the percentage was lower, albeit not significantly (∼30%, $P < 0.15$). Surprisingly, the percentage of peritoneal mast cells (PMCs) obtained from $Tpc1^{-/-}$ mice was significantly reduced by more than half compared to $Tpc1^{+/+}$ (from ∼5% to ∼2%) (Table 1 and Fig. 1*C*). We verified that TPC1 is indeed expressed in mast cells, using Western blotting of sorted $CD117^+$ PMCs (Fig. 1*D* and *SI Appendix*, Fig. S1 *B* and *C*). To examine whether the reduced number of mast cells is accompanied by changes in cell morphology, transmission electron microscopy (TEM) analysis was performed. Quantifying basic parameters of granules, such as size and number of granules, as well as vesicle density, revealed that PMCs extracted from $Tpc1^{-/-}$ mice displayed a similar morphology compared to $Tpc1^{+/+}$ PMCs (Fig. 1*E* and *SI Appendix*, Table S1) However, the overall size of $Tpc1^{-/-}$ PMCs was slightly reduced compared to $Tpc1^{+/+}$ counterparts (Fig. 1*F* and *SI Appendix*, Table S1).

Although passive systemic anaphylaxis (33), which is mainly arbitrated by mast cell- and basophil-mediated histamine release, was augmented in $Tpc1^{-/-}$ mice, the number and size of mast cells was significantly reduced (Table 1 and Fig. 1 *C* and *F*). Thus, we wondered whether $Tpc1^{-/-}$ mast cells showed enhanced histamine release, thereby explaining the observed phenotype. Therefore, we assessed basal histamine release of PMCs ex vivo. PMCs were cocultured with other peritoneal cells obtained from the lavage, as the latter provide essential cytokines and growth factors and thus improve the viability of PMCs (34). Finally, we calculated the average histamine content per PMC via cell lysis and normalization to $CD117^+$ mast cell counts in the lavage. Notably, $Tpc1^{-/-}$ PMCs contained significantly (almost 3 times, $^{***}P < 0.0001$) more histamine (∼3.4 ± 1.5 pg per cell) compared to $Tpc1^{+/+}$ PMCs (∼1.2 ± 0.6 pg per cell; Fig. 1 *G*, *Left*). Also, when looking at all cells of the peritoneal lavage, disregarding the reduced mast cell number of $Tpc1^{-/-}$ mice, basal secretion at rest was significantly enhanced in $Tpc1^{-/-}$ compared to $Tpc1^{+/+}$ cells (∼1.6-fold; Fig. 1 *G*, *Right*). Moreover, either by applying the sarco/ER Ca^{2+} ATPase (SERCA) inhibitor thapsigargin (TG) to induce Ca^{2+}-triggered secretion, or by stimulating G protein-dependent exocytosis using the synthetic secretagogue compound 48/80 (C48/80), histamine release was enhanced in $Tpc1^{-/-}$ peritoneal cells compared to $Tpc1^{+/+}$ cells (Fig. 1 *H* and *I*). These results are in line with the observed augmented anaphylaxis in TPC1-deficient mice in vivo (Fig. 1*A*). To elucidate, whether the degranulation of other mediators was altered in $Tpc1^{-/-}$ PMCs as well, we cultured isolated peritoneal cells for 2 wk in RPMI supplemented with interleukin-3 (IL-3) and stem cell factor (SCF) to enrich PMCs (33) and analyzed them for their β-hexosaminidase release (Fig. 1 *J*–*N*). β-Hexosaminidase is widely used as a measure for lysosomal degranulation, but is also present in almost all types of mast cell granules (35, 36). Similar to histamine release, β-hexosaminidase secretion was significantly enhanced in $Tpc1^{-/-}$ compared to $Tpc1^{+/+}$ PMCs in response to TG (Fig. 1*K*) and C48/80 (Fig. 1*L*) as well as physiological stimulation using a DNP-specific IgE antibody followed by antigen stimulation (Fig. 1*M*). However, basal β-hexosaminidase release was similar between the two genotypes (Fig. 1*J*), and, also, application of the ionophore ionomycin, triggering an instant increase in intracellular $[Ca^{2+}]$, yielded no differences between the two genotypes (Fig. 1*N*). This points to a role of TPC1 in mast cell degranulation processes.

Aside from mast cells, basophil granulocytes are also capable of releasing histamine and might contribute to the in vivo phenotype. Therefore, we utilized a rat basophil leukemia cell line (RBL-1) and measured their basal histamine release at rest as well as upon C48/80 stimulation. Notably, their histamine release was much lower (∼24% basal, ∼7% C48/80) compared to PMCs (*SI Appendix*, Fig. S1*E* and Fig. 1*G*). To elucidate whether the β-hexosaminidase secretion upon TPC1 inhibition was affected similarly in this cell type compared to $Tpc1^{-/-}$ PMCs, we applied the plant alkaloid tetrandrine (*Tet*), which has previously been described as an inhibitor of TPCs (27). Applying 500 nM *Tet* to

PHYSIOLOGY

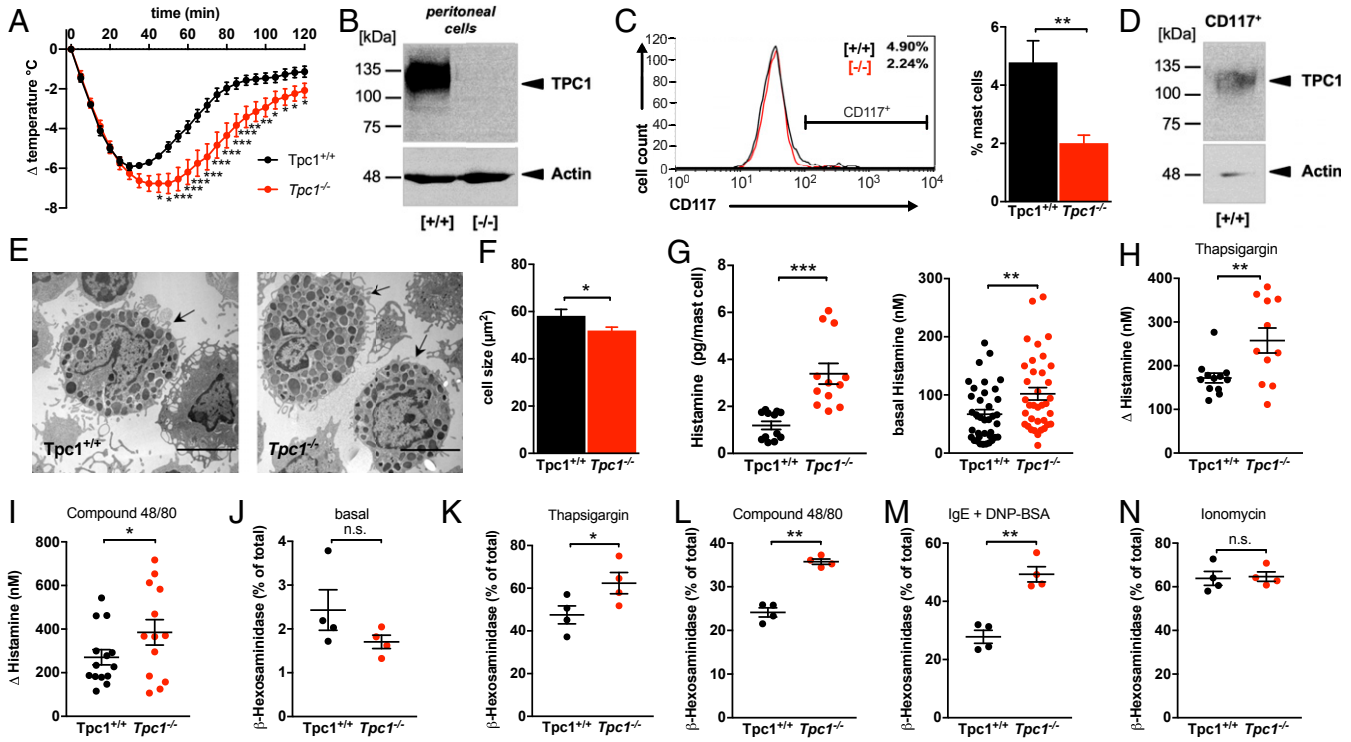

Fig. 1. TPC1 deficiency results in accelerated anaphylaxis and histamine release. (*A*) Time course of body temperature changes induced by an i.v. injection of DNP (2.7 mg/kg of body weight) in control mice (Tpc1$^{+/+}$, black) and mice lacking TPC1 (*Tpc1*$^{-/-}$, red). Mice were presensitized with IgE-αDNP (120 μg/kg of body weight) 24 h before DNP application; $n = 9$ mice per genotype. Graphics represent mean ± SEM. (*B*) Western blot (WB) analysis of cells isolated from the peritoneum of Tpc1$^{+/+}$ ([$^{+/+}$]) and *Tpc1*$^{-/-}$ ([$^{-/-}$]) mice. (*C*) Representative histogram overlay of Tpc1$^{+/+}$ ([$^{+/+}$], black) and *Tpc1*$^{-/-}$ ([$^{-/-}$], red) peritoneal cells (*Left*) expressing cell surface CD117 and statistical quantification (*Right*, $n = 4$ mice). (*D*) Identification of TPC1 in isolated CD117^{+} mast cells of Tpc1$^{+/+}$ mice by WB. (*E*) Representative TEM images of Tpc1$^{+/+}$ (*Left*, black arrow) and *Tpc1*$^{-/-}$ (*Right*, black arrows) PMCs. (Scale bars: 5 μm.) (*F*) Quantitative analysis of the cell size of Tpc1$^{+/+}$ and *Tpc1*$^{-/-}$ mast cells visualized in *E*; data are obtained from four animals per genotype with 21 cells each. Data are presented as average cell size (in square micrometers) ± SEM. (*G*) Basal histamine release of Tpc1$^{+/+}$ (black, $n = 11$ mice) and *Tpc1*$^{-/-}$ (red, $n = 11$ mice) mast cells. Calculation of average histamine content per PMC normalized to CD117^{+} cells (*Left*) and histamine release calculated in nanomolars measured in peritoneal lavage cell culture supernatants collected after 30 min of incubation (*Right*). Scattered blots depict mean ± SEM. Histamine release of Tpc1$^{+/+}$ (black) and *Tpc1*$^{-/-}$ (red) mast cells in the lavage in response to (*H*) TG ($n = 6$ mice) and (*I*) compound 48/80 ($n = 7$ mice) treatment for 30 min, shown as delta-histamine release on top of the basal release presented in *G*, *Right*. Scattered blots indicate mean ± SEM. (*J*) Basal β-hexosaminidase secretion in cultured primary mast cells of Tpc1$^{+/+}$ (black, $n = 4$ mice) and *Tpc1*$^{-/-}$ (red, $n = 4$ mice). β-Hexosaminidase secretion of cultured primary mast cells of Tpc1$^{+/+}$ (black, $n = 4$ mice) and *Tpc1*$^{-/-}$ (red, $n = 4$ mice) stimulated with (*K*) TG, (*L*) compound 48/80, (*M*) IgE (overnight) and DNP-BSA (100 ng/mL), and (*N*) ionomycin for 30 min. Scattered blots indicate mean ± SEM; n.s. (not significant), *$P < 0.05$, **$P < 0.01$, ***$P < 0.001$ (two-tailed Student's *t* test).

Tpc1$^{+/+}$ PMCs or RBL-1 cells for 45 min did not affect basal β-hexosaminidase release, compared to controls (*SI Appendix*, Fig. S1 *D* and *F*). Pharmacological TPC1 inhibition, however, further enhanced IgE-triggered β-hexosaminidase release significantly in both Tpc1$^{+/+}$ PMCs and RBL-1 cells (*SI Appendix*, Fig. S1 *D* and *F*). Thus, TPC1 is essential for mediator secretion in primary mast cells and a basophil leukemia cell line.

TPC1 Deficiency Results in Enhanced Mast Cell Degranulation. To investigate whether G protein-induced degranulation was altered in primary *Tpc1*$^{-/-}$ mast cells, we directly determined the fusion of mast cell granules to the plasma membrane using whole-cell patch clamp (34, 37). Applying this technique, we first determined the initial cell surface area for Tpc1$^{+/+}$ and *Tpc1*$^{-/-}$ PMCs (Fig. 2*A*). The capacitance recordings confirmed our primary morphological analysis (Fig. 1*F*) and indicate that *Tpc1*$^{-/-}$ mast cells are significantly smaller than Tpc1$^{+/+}$ cells (Fig. 2*A*). To mimic G protein-induced degranulation, GTPγS was applied via the patch pipette. Fig. 2*B* illustrates the increase in cell area of a PMC before and after the degranulation response. In line with the increased histamine release (Fig. 1 *G*–*I*) and enhanced β-hexosaminidase secretion (Fig. 1 *K*–*M*), *Tpc1*$^{-/-}$ mast cells showed enhanced GTPγS-induced degranulation responses compared to Tpc1$^{+/+}$ cells (Fig. 2 *C*, *Left*). The degranulation amplitude after 300 s was significantly increased in *Tpc1*$^{-/-}$ mast cells (Fig. 2 *C*, *Right*).

To test whether pharmacological modulation of TPC1 mimics the *Tpc1*$^{-/-}$ phenotype, we next applied the TPC1 inhibitor *Tet*. Treatment of Tpc1$^{+/+}$ PMCs with 500 nM *Tet* for 15 min did not affect cell surface area (Fig. 2*D*), thereby excluding a potential overestimation of the observed effects. However, if Tpc1$^{+/+}$ mast cells were pretreated with *Tet* and subsequently stimulated with GTPγS, as described above, *Tet* was able to reproduce the

Table 1. Distribution of distinct immune cells within the peritoneal lavage

	Tpc1$^{+/+}$	*Tpc1*$^{-/-}$
T cells (%)	6.51 ± 1.43	6.47 ± 1.06
B cells (%)	26.69 ± 4.00	29.23 ± 2.84
Macrophages (%)	40.64 ± 6.21	30.38 ± 2.38
Mast cells (%)	4.78 ± 0.73	2.01 ± 0.27**
Neutrophils (%)	1.32 ± 0.23	1.92 ± 0.37

Note a significant reduction of CD117^{+} mast cells extracted from *Tpc1*$^{-/-}$ mice. Data are mean values ± SEM. **$P < 0.01$ (two-tailed Student's *t* test).

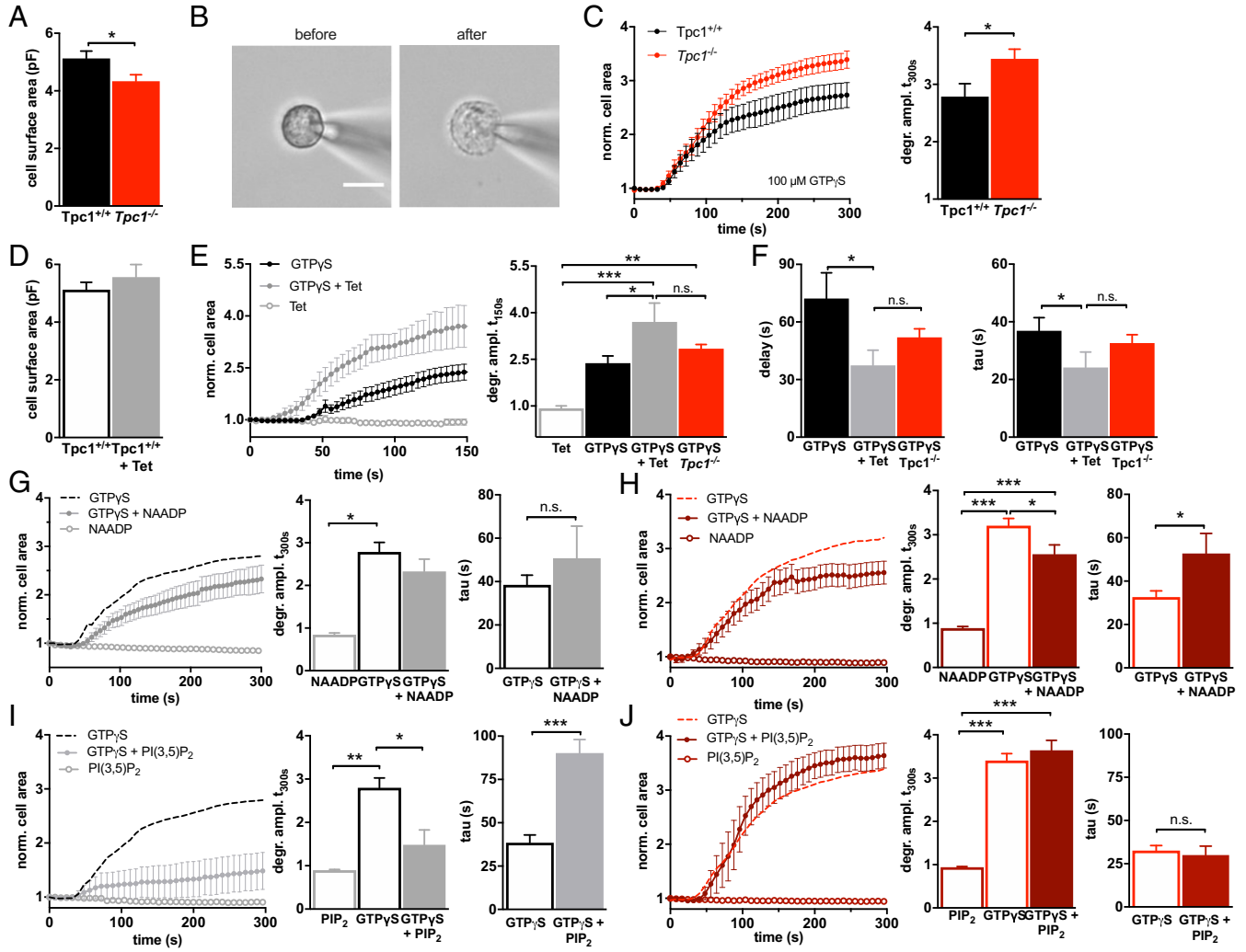

Fig. 2. TPC1 activity dampens G protein-triggered mast cell degranulation. (*A*) Electrophysiological measurements of membrane capacitance via the whole-cell patch clamp technique as an estimate of cell surface area (in picofarads) were used to record mast cell degranulation. Initial capacitance was measured immediately after whole-cell break-in. Surface areas of mast cells derived from Tpc1$^{+/+}$ (black, $n = 23$) and *Tpc1*$^{-/-}$ (red, $n = 26$) mice were averaged and depicted as mean ± SEM. *$P < 0.05$ (two-tailed Student's *t* test). (*B*) Representative mast cell before (*Left*) and after degranulation (*Right*). (Scale bar: 10 µm.) (*C*) Average normalized capacitance measurements of GTPγS-induced exocytosis (100 µM) in Tpc1$^{+/+}$ (black, $n = 20$) and *Tpc1*$^{-/-}$ (red, $n = 26$) mast cells. Capacitance was measured every 2 s, and the initial capacitance determined immediately after whole-cell break-in was used to normalize subsequent values (*Left*). Data were averaged and blotted versus time in seconds as mean ± SEM. Degranulation amplitudes from Tpc1$^{+/+}$ (black, $n = 20$) and *Tpc1*$^{-/-}$ (red, $n = 26$) mast cells were extracted at 300 s, averaged, and depicted as mean ± SEM (*Right*). *$P < 0.05$ (two-tailed Student's *t* test). (*D*) Initial capacitance was measured immediately after whole-cell break-in. Tpc1$^{+/+}$ mast cells were pretreated with (gray bar, $n = 12$) or without (black open bar; taken from *A*, $n = 23$) the TPC inhibitor *Tet* (0.5 µM) for 15 min. Surface areas of mast cells were averaged and depicted as mean ± SEM. (*E*) Capacitance measurements were acquired and analyzed as in *C*. Tpc1$^{+/+}$ mast cells were pretreated with or without *Tet* (0.5 µM) for 15 min and stimulated with *GTP*γS (100 µM) (black circles, $n = 19$), *GTP*γS + *Tet* (gray solid circles, $n = 12$), or *Tet* alone (gray open circles, $n = 5$) (*Left*). Degranulation amplitudes of *GTP*γS-perfused Tpc1$^{+/+}$ mast cells with (gray bar, $n = 12$) or without (black bar, $n = 19$) *Tet*, as well as from *GTP*γS-treated *Tpc1*$^{-/-}$ mast cells (red bar, $n = 26$) and *Tet* alone (gray, open bar, n = 5) were extracted at 150 s, averaged, and depicted as mean ± SEM. *$P < 0.05$, **$P < 0.01$, ***$P < 0.0001$ (one-way ANOVA) (*Right*). (*F*) Analysis of the delay (*Left*) and rate of release (tau) (*Right*) assessed from the data in *C* and *E*. *$P < 0.05$ (one-way ANOVA). (*G* and *H*) Capacitance measurements were acquired and analyzed as in *C*. (*G*) Tpc1$^{+/+}$ and (*H*) *Tpc1*$^{-/-}$ mast cells stimulated with *GTP*γS (100 µM) were pretreated with *GTP*γS + NAADP (Tpc1$^{+/+}$: gray, $n = 12$; *Tpc1*$^{-/-}$: dark red, $n = 16$) or without *GTP*γS (Tpc1$^{+/+}$: black open, $n = 19$; *Tpc1*$^{-/-}$: red open, $n = 26$, taken from *C*) the TPC1 activator NAADP (1 µM) or with NAADP alone (Tpc1$^{+/+}$: gray open, $n = 5$; *Tpc1*$^{-/-}$: dark red open, $n = 5$) (*Left*). Degranulation amplitudes of mast cells were extracted at 300 s, averaged, and depicted as mean ± SEM (*Middle*). *$P < 0.05$, **$P < 0.01$, ***$P < 0.0001$ (one-way ANOVA). Analysis of the delay and rate of release (tau) assessed from the data in *G*, *H*, and *C* (*Right*). Data are depicted as mean ± SEM. *$P < 0.05$ (two-tailed Student's *t* test). (*I* and *J*) Capacitance measurements were acquired and analyzed as in *G* and *H*. (*I*) Tpc1$^{+/+}$ and (*J*) *Tpc1*$^{-/-}$ mast cells stimulated with *GTP*γS (100 µM) were pretreated with *GTP*γS + PIP_2 (Tpc1$^{+/+}$: gray, $n = 5$; *Tpc1*$^{-/-}$: dark red, $n = 5$) or without *GTP*γS (Tpc1$^{+/+}$: black open, $n = 20$; *Tpc1*$^{-/-}$: red open, $n = 26$, taken from *C*) the TPC1 activator PI(3,5)P_2 (10 µM) or with PI(3,5)P_2 alone PIP_2 (Tpc1$^{+/+}$: gray open, $n = 5$; *Tpc1*$^{-/-}$: dark red open, $n = 5$) (*Left*). Degranulation amplitudes of mast cells were extracted at 300 s, averaged, and depicted as mean ± SEM (*Middle*). *$P < 0.05$, **$P < 0.01$, ***$P < 0.0001$ (one-way ANOVA). Analysis of the delay and rate of release (tau) assessed from the data in *I*, *J*, and *C* (*Right*). Data are depicted as mean ± SEM. ***$P < 0.001$ (two-tailed Student's *t* test).

degranulation phenotype observed for *Tpc1*$^{-/-}$ PMCs upon stimulation: While it did not affect degranulation on its own, *Tet* increased the mean degranulation amplitude after 150 s significantly (Fig. 2*E*). We further analyzed the kinetics of the response via curve fitting using a capacitance fit function (see *Materials and Methods*). This analysis revealed that the onset, indicated by the delay of the response (Fig. 2 *F*, *Left*), and the kinetics, estimated by the rate of release (*tau*) (Fig. 2 *F*, *Right*), were both significantly reduced in *Tet*-pretreated Tpc1$^{+/+}$ PMCs compared to control cells and similar to *Tpc1*$^{-/-}$ PMCs. Thus, our results indicate a faster and enhanced mast cell degranulation after either genetic ablation or pharmacological inhibition of TPC1 (Fig. 2 *C*–*F*).

Accordingly, we asked whether activation of TPC1 would induce or mitigate mast cell degranulation responses. Therefore, we first applied the second messenger NAADP (1 μM) via the patch pipette, thus directly or indirectly activating endogenous TPC1 channels (18). Notably, NAADP alone did not induce degranulation in Tpc1$^{+/+}$ PMCs, but its coapplication slightly reduced GTPγS-induced degranulation responses (Fig. 2*G*). However, NAADP also affected GTPγS-induced degranulation in *Tpc1*$^{-/-}$ PMCs (Fig. 2*H*) in a similar manner, although the difference for NAADP alone remained significant (Fig. 2 *H*, *Right*). This suggests the involvement of other NAADP-dependent mechanisms in the degranulation of *Tpc1*$^{-/-}$ PMCs. Similar to NAADP, the known TPC activator PI(3,5)P_2 (22–24) alone also did not induce degranulation in wild-type PMCs, indicating that TPCs might not be expressed in secretory granule membranes. However, when applied simultaneously with GTPγS, degranulation amplitude as well as tau were significantly reduced (Fig. 2*I*). Evidently, coapplication of PI(3,5)P_2 with GTPγS did not affect GTPγS-induced degranulation responses in TPC1-deficient PMCs (Fig. 2*J*), signifying no effect of TPC2 in the degranulation processes. To further ensure that TPC2 was not contributing to our observed phenotype, we utilized a *Tpc2*$^{-/-}$ mouse line (26) and triggered exocytosis analogously via perfusion with GTPγS. Interestingly, TPC2 deficiency did not trigger significant alterations in the initial cell surface area (*SI Appendix*, Fig. S1*G*), the degranulation amplitude, or the kinetics (*SI Appendix*, Fig. S1*H*). Therefore, our results suggest that TPC1 is a crucial regulator of mast cell degranulation, directly affecting kinetic and efficiency of vesicle fusion, possibly by modifying the necessary local Ca^{2+} increase.

IgE-Dependent Ca^{2+} Signaling Is Enhanced in *Tpc1*$^{-/-}$ Mast Cells. TPCs have been implicated in Ca^{2+} signaling and homeostasis (18), and Ca^{2+} is essential for mast cell exocytosis and secretion (8). Therefore, differences in basal intracellular Ca^{2+} concentrations ($[Ca^{2+}]_i$) could contribute to the hypersecretory phenotype of *Tpc1*$^{-/-}$ PMCs. However, basal $[Ca^{2+}]_i$ were comparable between the two genotypes (*SI Appendix*, Fig. S2*A*), hinting toward altered degranulation processes.

Mast cells are classically activated via IgE-dependent cross-linking of high affinity $F_c\varepsilon$ receptors (13), and IgE/DNP stimulation demonstrated the strongest β-hexosaminidase release (Fig. 1*M* and *SI Appendix*, Fig. S1*D*). This process results in IP_3 production, followed by a sustained increase in cytosolic Ca^{2+} concentrations. As TPC1 has been implicated in the release of Ca^{2+} from acidic granules (17, 18, 28), we next investigated whether IgE-induced Ca^{2+} signals were altered in *Tpc1*$^{-/-}$ PMCs. Therefore, analogous to our in vivo and β-hexosaminidase degranulation experiments, we pretreated *Tpc1*$^{-/-}$ and Tpc1$^{+/+}$ PMCs overnight with IgE specific for DNP and, subsequently, triggered cross-linking using the respective antigen (Fig. 3). In the presence of 2 mM extracellular Ca^{2+}, the IgE-induced intracellular Ca^{2+} signal was faster in *Tpc1*$^{-/-}$ compared to Tpc1$^{+/+}$ PMCs and significantly different at 90 s, while it reached similar amounts around 300 s, indicating potential differences in the Ca^{2+} release rather than influx (Fig. 3*A*). Calculating the area under the curve (AUC) as a measure of total Ca^{2+} released over time, $[Ca^{2+}]_i$, we observed significantly exaggerated responses in *Tpc1*$^{-/-}$ compared to Tpc1$^{+/+}$ mast cells (Fig. 3*B*) Consequently, as TPCs are localized to the endolysosomal compartment, we next concentrated on Ca^{2+} signals that originate from intracellular Ca^{2+} stores, by omitting Ca^{2+} from the extracellular solution. Fig. 3*C* illustrates that *Tpc1*$^{-/-}$ PMCs displayed enhanced Ca^{2+} release from intracellular stores upon $F_c\varepsilon$R cross-linking. Analyzing the peak of release at 125 s, we found that *Tpc1*$^{-/-}$ PMCs had a significantly higher increase in cytosolic Ca^{2+} levels compared to Tpc1$^{+/+}$ (Fig. 3 *C*, *Right*). Calculating the AUC, we again detected significantly amplified responses in *Tpc1*$^{-/-}$ compared to Tpc1$^{+/+}$ mast cells (Fig. 3*D*), in line with our previous findings (Fig. 1 *A* and *H*–*N*).

As TPC1 inhibition with *Tet* significantly enhanced GTPγS-induced degranulation (Fig. 2 *E* and *F*), we inquired whether inhibition of TPC activity in wild-type cells would resemble the *Tpc1*$^{-/-}$ phenotype with respect to IgE/$F_c\varepsilon$R-triggered Ca^{2+} signals. As expected, pretreatment of Tpc1$^{+/+}$ mast cells with *Tet* (500 nM) for 15 min, followed by IgE/$F_c\varepsilon$R stimulation, resulted in a similar Ca^{2+} release rate (Fig. 3 *E* and *F*) with similar peak Ca^{2+} concentrations at 125 s (Fig. 3 *E*, *Right*) compared to *Tpc1*$^{-/-}$ mast cells. Although the overall Ca^{2+} influx over time did not completely resemble the *Tpc1*$^{-/-}$ phenotype, it was significantly different than that observed in Tpc1$^{+/+}$ mast cells (Fig. 3*F*). To further link our phenotype to TPC1 activity, we also preincubated the cells with a different TPC inhibitor, *trans*-Ned-19 (38), antagonizing NAADP stimulation, for 15 min (*Ned19*, 1 μM) (Fig. 3 *G* and *H*). Similar to the results obtained with *Tet*, the inhibition of TPCs using *trans*-Ned-19 also converted the shape of the IgE-induced Ca^{2+} signals in Tpc1$^{+/+}$ to *Tpc1*$^{-/-}$ mast cells (Fig. 3*G*). The overall Ca^{2+} influx over time completely resembled the *Tpc1*$^{-/-}$ phenotype and was significantly different than that observed in Tpc1$^{+/+}$ mast cells (Fig. 3*H*). Thus, TPC1 appears to be essential for organellar Ca^{2+} homeostasis and regulated receptor-operated Ca^{2+} release.

TPC1 Differentially Regulates the Ca^{2+} Storage Capacity of Intracellular Organelles. To identify the intracellular compartment from which Ca^{2+} is released upon IgE stimulation, we applied the cathepsin C substrate glycyl-L-phenylalanine-beta-naphthylamide (GPN), which is thought to specifically disrupt endolysosomal membranes, thereby leading to a selective leakage of endolysosomal Ca^{2+} (39). Surprisingly, *Tpc1*$^{-/-}$ mast cells showed significantly reduced Ca^{2+} signals originating from the endolysosomal compartment, compared to Tpc1$^{+/+}$ PMCs (Fig. 4*A*). Quantification of the fluorescence intensity after 350 s (Fig. 4 *A*, *Middle*) and calculation of the Ca^{2+} influx over time (Fig. 4 *A*, *Right*) also confirmed a significant difference in *Tpc1*$^{-/-}$ and Tpc1$^{+/+}$ endolysosomal storage capacity. Therefore, a substantial contribution of endolysosomal Ca^{2+} could be excluded as a source of the accelerated IgE-induced rise in $[Ca^{2+}]_i$ in *Tpc1*$^{-/-}$ mast cells (Fig. 3 *C*–*H*). Thus far, our results indicate that Ca^{2+} homeostasis in acidic organelles is directly or indirectly dependent on TPC1.

To find the source of the elevated Ca^{2+} efflux in *Tpc1*$^{-/-}$ mast cells, we assessed the contribution of the ER, the largest intracellular Ca^{2+} store, using the SERCA inhibitor TG. Primary TPC1-deficient PMCs indeed displayed enhanced intracellular Ca^{2+} signals upon TG stimulation compared to wild-type cells (*SI Appendix*, Fig. S2*B*). This finding was supported by pharmacological inhibition of TPCs using *Tet* in RBL-1 cells (*SI Appendix*, Fig. S2*C*). To monitor the ER-Ca^{2+} content ($[Ca^{2+}]_{ER}$) (40) directly, we employed the low-affinity Ca^{2+} indicator Fura-2-FF ($K_D \approx 10$ μM) (41). Interestingly, significantly higher Ca^{2+} levels were detected in the ER of resting *Tpc1*$^{-/-}$

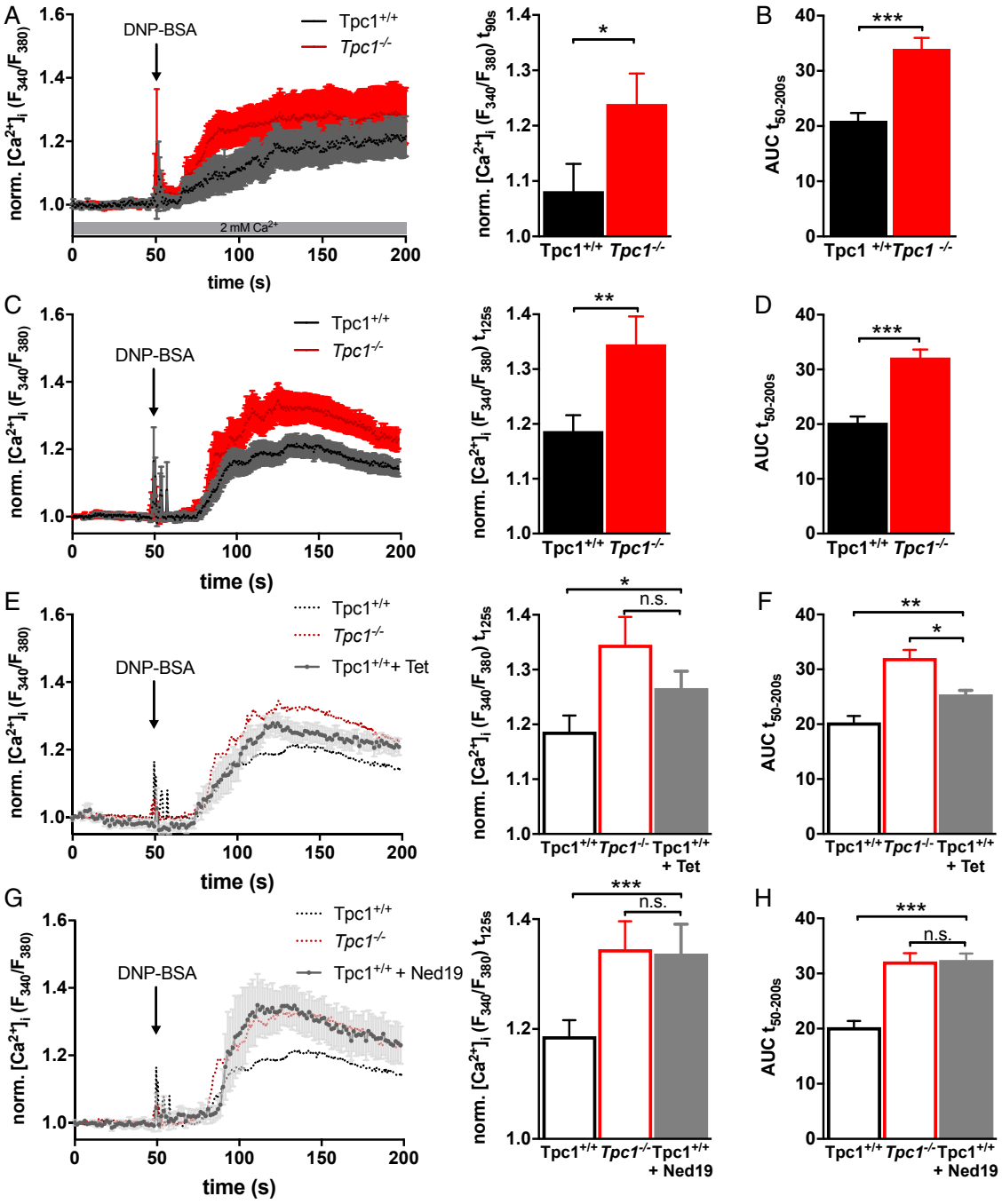

Fig. 3. TPC1 affects IgE-dependent Ca^{2+} signaling via regulation of the Ca^{2+} homeostasis between different intracellular stores. (*A*) Ratiometric Fura-2 AM-dependent measurements of cytosolic Ca^{2+} concentrations in the presence of 2 mM $[Ca^{2+}]_e$. $Tpc1^{+/+}$ (black, $n = 19$) and $Tpc1^{-/-}$ (red, $n = 23$) mast cells were pretreated with DNP-specific IgE antibodies (100 ng/mL) overnight and stimulated with 100 ng/mL DNP-BSA at 50 s (arrow). Data were normalized to the initial F_{340}/F_{380} ratio, averaged, and blotted versus time as mean ± SEM (*Left*). Bar graphs show mean peak cytosolic Ca^{2+} concentrations at 90 s extracted from *A* ± SEM (*Right*). $^*P < 0{,}05$ (two-tailed Student's *t* test). (*B*) Quantification of the AUC was used as an estimate of the total increase in the cytosolic Ca^{2+} concentration over time. Data are shown as mean ± SEM. $^{***}P < 0{,}001$ (two-tailed Student's *t* test). (*C*) Ratiometric Fura-2 AM-dependent measurements of cytosolic Ca^{2+} concentrations in the absence of $[Ca^{2+}]_e$ (0.5 mM EGTA) (*Left*). $Tpc1^{+/+}$ (black, $n = 36$) and $Tpc1^{-/-}$ (red, $n = 27$) mast cells were treated as in *A*. Data were normalized to the initial F_{340}/F_{380} ratio, averaged, and blotted versus time as mean ± SEM. Bar graphs show mean peak cytosolic Ca^{2+} concentrations at 125 s extracted from *C* ± SEM (*Right*). $^{**}P < 0{,}01$ (two-tailed Student's *t* test). (*D*) Quantification of the AUC was used as an estimate of the total increase in the cytosolic Ca^{2+} concentration over time. Data are shown as mean ± SEM. $^{***}P < 0{,}001$ (two-tailed Student's *t* test). (*E*) $Tpc1^{+/+}$ mast cells were preincubated with *Tet* for 15 min prior to DNP-BSA stimulation; cytosolic Ca^{2+} signals were acquired and analyzed as in *A*. Traces from *C* are depicted as dashed lines, for better comparison (*Left*). Mean peak cytosolic Ca^{2+} concentrations at 125 s extracted from *Left* (gray, solid bar) and as comparison peak levels from *C* (open bars) (*Right*). (*F*) Average AUC calculated from *E* (gray, solid bar) and as comparison from *D* (open bars) ± SEM. $^*P < 0.05$, $^{**}P < 0.01$ (one-way ANOVA). (*G*) $Tpc1^{+/+}$ mast cells were preincubated with *trans*-Ned-19 for 15 min prior to DNP-BSA stimulation; cytosolic Ca^{2+} signals were acquired and analyzed as in *C*. Traces from *C* are depicted as dashed lines, for better comparison (*Left*). Mean peak cytosolic Ca^{2+} concentrations at 125 s extracted from *Left* (gray, solid bar) and as comparison peak levels from *C* (open bars) (*Right*). (*H*) Average AUC calculated from *G* (gray, solid bar) and as comparison from *D* (open bars) ± SEM. $^{***}P < 0.001$ (one-way ANOVA).

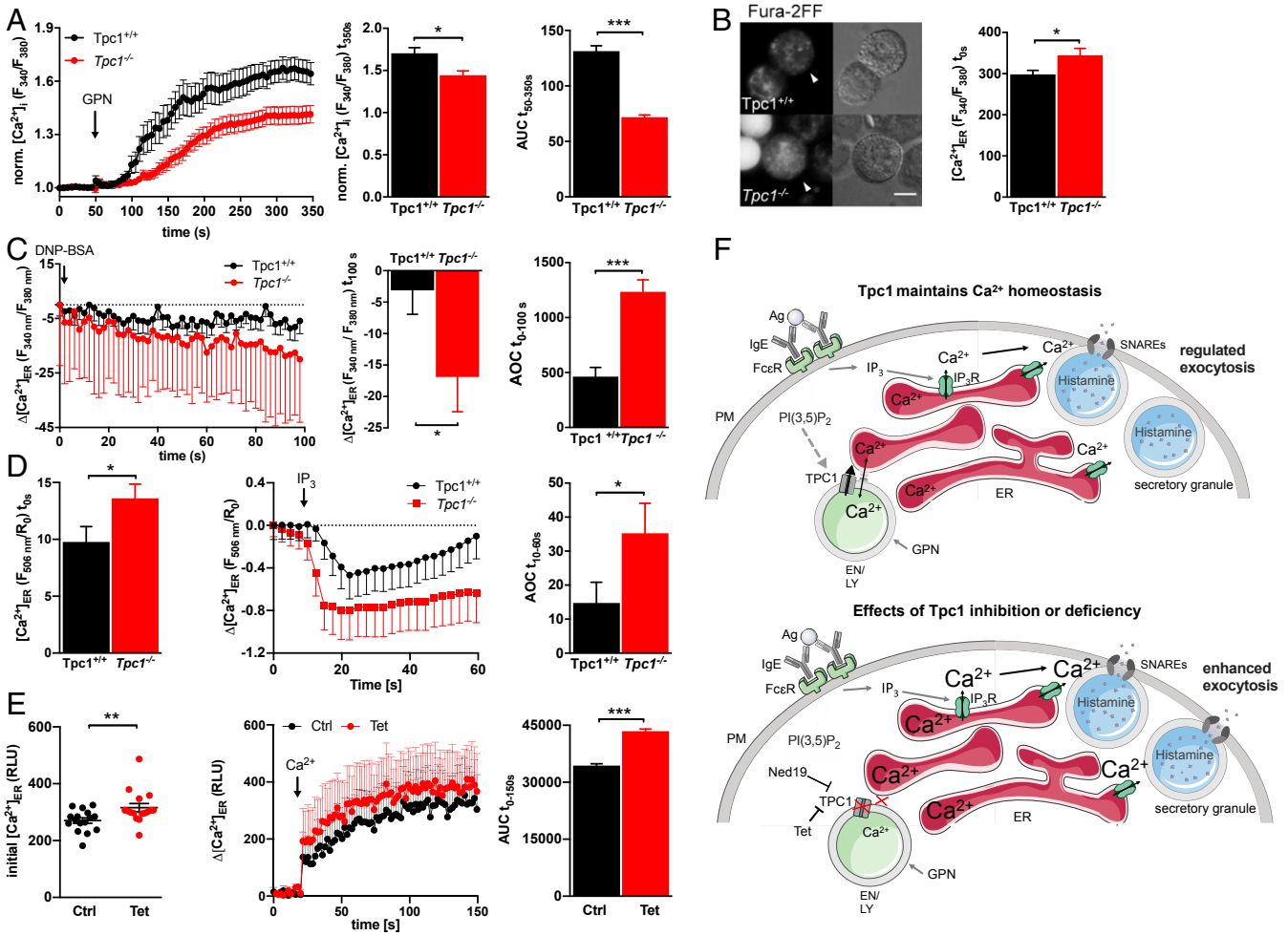

Fig. 4. TPC1-deficient mast cells exhibit higher ER-Ca^{2+} concentrations and stronger ER-Ca^{2+} signals. (*A*) Measurements of cytosolic Ca^{2+} concentrations (Fura-2 AM) in $Tpc1^{+/+}$ (black, $n = 62$) and $Tpc1^{-/-}$ (red, $n = 32$) mast cells stimulated with 100 μM GPN at 50 s (arrow). Data were normalized to the initial F_{340}/F_{380} ratio, averaged, and blotted versus time of the experiment as mean ± SEM. Bar graphs of mean peak cytosolic Ca^{2+} concentrations at 350 s extracted from *A* ± SEM (*Middle*). Average AUC ± SEM (*Right*). $*P < 0.05$, $***P < 0.0001$ (two-tailed Student's *t* test). (*B*) Ratiometric Fura-2-FF AM-dependent measurements of Ca^{2+} concentrations in the intracellular stores. Representative confocal laser scanning microscopic images of $Tpc1^{+/+}$ and $Tpc1^{-/-}$ mast cells loaded with Fura-2-FF AM for 45 min (*Left*). (Scale bar: 5 μm.) Quantification of resting Ca^{2+} concentrations in the Ca^{2+}-stores of $Tpc1^{+/+}$ (black, $n = 49$) and $Tpc1^{-/-}$ (red, $n = 38$) mast cells (*Right*). Bars show mean ± SEM $*P < 0.05$ (two-tailed Student's *t* test). (*C*) Average traces of the Ca^{2+} release out of Ca^{2+} stores of $Tpc1^{+/+}$ (black, $n = 17$) and $Tpc1^{-/-}$ (red, $n = 17$) mast cells in response to $F_{c\varepsilon}R$ cross-linking upon IgE binding and DNP-BSA stimulation. To visualize the Ca^{2+} released from the ER, the initial $[Ca^{2+}]_{ER}$ were subtracted and blotted as delta $[Ca^{2+}]_{ER}$ ($\Delta[Ca^{2+}]_{ER}$) versus time (in seconds; *Left*). Quantification of the Ca^{2+} released at 100 s from $Tpc1^{+/+}$ (black, $n = 17$) and $Tpc1^{-/-}$ (red, $n = 17$) mast cells (*Middle*). Data were averaged and blotted as mean ± SEM. Quantification of the Ca^{2+} released from the ER over time, via calculation of the AOC from 0 s to 100 s (*Right*). Data are shown as mean AOC ± SEM, $*P < 0.05$, $**P < 0.001$ (two-tailed Student's *t* test). (*D*) Quantification of resting Ca^{2+} concentrations using Mag-Fluo-4 AM in the Ca^{2+} stores of permeabilized $Tpc1^{+/+}$ (black, $n = 49$) and $Tpc1^{-/-}$ (red, $n = 38$) mast cells (*Left*). Average traces of the Ca^{2+} release out of Ca^{2+} stores of $Tpc1^{+/+}$ (black, $n = 14$) and $Tpc1^{-/-}$ (red, $n = 17$) mast cells in response to IP_3 stimulation. To visualize the Ca^{2+} released from the ER, the initial $[Ca^{2+}]_{ER}$ were subtracted and blotted as delta $[Ca^{2+}]_{ER}$ ($\Delta[Ca^{2+}]_{ER}$) versus time (in seconds; *Middle*). Data were averaged and blotted as mean ± SEM. Quantification of the Ca^{2+} released from the ER over time, via calculation of the AOC from 10 s to 60 s (*Right*). Data are shown as mean AOC ± SEM. Bars show mean ± SEM. $*P < 0.05$ (two-tailed Student's *t* test). (*E*) RBL-1 cells transfected with an ER-tagged aequorine construct (ER-2mutAEQ, Addgene) were utilized to monitor $[Ca^{2+}]_{ER}$. Cells were treated with (red, $n = 16$) or without (black, $n = 16$) *Tet* to inhibit TPC1 channels for 2.5 h. Averaged initial $[Ca^{2+}]_{ER}$ (*Left*). Refilling with Ca^{2+} (2 mM) after store depletion using the reversible SERCA inhibitor CPA (*Middle*). Data were averaged and blotted versus time as mean ± SEM. Quantification of the Ca^{2+} released from the ER over time, via calculation of the AUC from 0 s to 150 s (*Right*). Data are shown as mean AUC ± SEM. $**P < 0.001$, $***P < 0.0001$ (two-tailed Student's *t* test). (*F*) Working model: Illustrating the role of TPC1 in organellar Ca^{2+} homeostasis and IgE-induced exocytosis. TPCs, located in endolysosomal membranes, contribute to the maintenance of cellular Ca^{2+} homeostasis via facilitating the buffering capacity of these organelles (*Upper*). Upon $F_{c\varepsilon}$ receptor ($F_{c\varepsilon}R$) stimulation and subsequent phospholipase C activation, formation of IP_3 triggers the release of Ca^{2+} by gating IP_3 receptors (IP_3R). In close proximity to the ER membrane, the release of Ca^{2+} mediated by TPC1 from endolysosomes causes a feed-forward loop, enhancing Ca^{2+} release from the ER and, at the same time, enabling the uptake of Ca^{2+} by endolysosomes (i.e., via facilitating the formation of contact sites). Activation of TPC1 by $PI(3,5)P_2$, however, depletes the lysosomal stores from Ca^{2+} thereby mimicking a TPC1-deficient phenotype. If the Ca^{2+} buffering capacity of the endolysosomal system controlled by TPC1 is missing or blocked by *Tet* or trans-NED-19 (*Ned19*) (*Lower*), the resting ER-Ca^{2+} concentration increases, causing elevated Ca^{2+} signals upon IP_3R activation, while reducing the uptake into lysosomes due to missing contact sites between the ER and endolysosomes. These higher ER-Ca^{2+} concentrations subsequently lead to elevated Ca^{2+} signals upon IP_3R activation and consequently enhanced exocytosis.

mast cells compared to Tpc1$^{+/+}$ controls (Fig. 4*B*). When triggering the release of Ca^{2+} from the ER using IgE/$F_c\varepsilon$R stimulation, we found that the drop in $[Ca^{2+}]_{ER}$ was more pronounced in *Tpc1*$^{-/-}$ mast cells compared to Tpc1$^{+/+}$ (Fig. 4*C*). To corroborate these results, we utilized another low-affinity Ca^{2+} indicator, Mag-Fluo-4 ($K_D \approx 22$ μM) (42). Therefore, we permeabilized the cells using digitonin (16 μM), thus preventing contamination due to cytosolic dye recognizing magnesium fluctuations (Fig. 4*D* and *SI Appendix*, Fig. S2 *D* and *E*). Similar to Fura-2-FF measurements, also monitoring $[Ca^{2+}]_{ER}$ via Mag-Fluo-4 demonstrated higher basal concentrations in TPC1-deficient mast cells (Fig. 4 *D*, *Left*) as well as in RBL-1 cells treated with *Tet* (*SI Appendix*, Fig. S2*D*). Upon stimulation of the IP_3R using IP_3, both TPC1-deficient mast cells (Fig. 4 *D*, *Middle*) and *Tet*-treated RBL-1 cells (*SI Appendix*, Fig. S2 *E*, *Left*) exhibited a more severe drop in $[Ca^{2+}]_{ER}$, resulting in significantly enhanced areas over the curve (AOCs) (Fig. 4*D* and *SI Appendix*, Fig. S2 *E*, *Right*). Altogether, our results suggest that the ER stores significantly more Ca^{2+}, once TPC1 is ablated or blocked. In order to strengthen this concept, we also employed an ER-tagged genetically encoded Ca^{2+} indicator (ER-2mutAEQ) (43, 44) and demonstrated that, upon TPC1 inhibition, refilling of the ER-Ca^{2+} store is indeed significantly enhanced in transiently transfected RBL-1 cells (Fig. 4*E*). Using the SERCA-inhibitor cyclopiazonic acid (CPA), which binds at the same site as TG, but is reversible, we depleted the ER stores from Ca^{2+} in Ca^{2+}-free media and refilled them by adding 2 mM Ca^{2+} (Fig. 4*E*). Inhibition of TPC1 channels using *Tet* resulted in significantly higher $[Ca^{2+}]_{ER}$ after depletion with CPA for 15 min (Fig. 4 *E*, *Left*) as well as in a significantly stronger increase in $[Ca^{2+}]_{ER}$ after readdition of Ca^{2+} (Fig. 4 *E*, *Right*). Thus, the refilling of the ER-Ca^{2+} stores is accelerated upon TPC1 inhibition in RBL-1 cells.

In summary, our results suggest an essential mechanism as to how TPC1 contributes to the maintenance of intracellular Ca^{2+} homeostasis and Ca^{2+} signaling (Fig. 4*F*), thereby controlling mast cell reactivity in vivo and ex vivo.

Discussion

In the present study, we identify the TPC protein TPC1 as a key element for regulated allergic and anaphylactic reactions. TPC1 deficiency in mice leads to exaggerated passive systemic anaphylaxis, resulting in a more severe temperature drop following allergen challenge. Deciphering the underlying molecular mechanism, we propose that TPC1 channel activity regulates organellar Ca^{2+} homeostasis, granular histamine content, Ca^{2+} signaling, and, thus, reactivity of murine mast cells and basophils. Our results show that TPC1-deficient mice exhibit fewer mast cells, yet are characterized by enhanced exocytosis and mediator release due to increased IgE/$F_c\varepsilon$R-triggered Ca^{2+} responses, resulting from altered filling of ER and organelle Ca^{2+} stores.

Herein, we present a report linking TPC1 activity with immune cell function in vivo. Global deletion of TPC1 in mice results in selectively reduced mast cell numbers in the peritoneum, while lymphocyte counts were unaffected. TPC1 depletion resulted not only in lower PMC numbers but also in reduced cell size, both of which could be compensatory measures in response to increased histamine contents in preformed secretory granules. One possibility could be that mature *Tpc1*$^{-/-}$ PMCs degranulate spontaneously to the extent that they cannot recover, resulting in faster cell turnover. *Tpc1*$^{-/-}$ PMCs may be smaller because they are still not fully matured. The histamine release rate was increased by more than ~4 times, while the cellular histamine content was only 3 times higher in *Tpc1*$^{-/-}$ compared to Tpc1$^{+/+}$ PMCs. In line with this observation, β-hexosaminidase secretion was enhanced in *Tpc1*$^{-/-}$ compared to Tpc1$^{+/+}$ PMCs in response to various stimuli, although the basal enzyme release was similar between the two genotypes. Thus, additional mechanisms involved in exocytosis seem to be altered. This notion was confirmed using pharmacological inhibition of TPC1 in a rat basophilic leukemia cell line, suggesting that basophils similar to mast cells amplify their mediator release upon TPC1 blockade.

Previously, TPCs have been shown to mediate exocytosis of primary human cytotoxic CD8$^+$ T cells (CTLs) in an NAADP-dependent manner, which the authors linked to TPC activation (28). While NAADP targeted acidic organelles in primary CTLs (28), it had no effect on endolysosomal Ca^{2+} release in a human CD4$^+$ Jurkat T cell line (45), suggesting that CD8$^+$ CTLs differ from CD4$^+$ helper T cells in their mediator release. Although secretory lysosome biogenesis is similar to the biogenesis of conventional lysosomes in CTLs and mast cells (45), the latter cells are unique in that they contain several distinct lysosome-related secretory granules with different contents and relying on diverse exocytic mechanisms (46, 47). While TPCs are located in acidic granule membranes and were found in lytic granule membranes of CTLs (28), it is not clear, to date, whether they are also present in mast cell granules. However, as the TPC agonists $PI(3,5)P_2$ and NAADP were themselves unable to trigger degranulation in mast cells, our results point to different mechanisms underlying mast cell granule fusion compared to CTLs, suggesting a diverse distribution pattern of TPC1 in distinct cellular organelles.

Mast cells release their numerous secretory granules in response to different immunological triggers, most of which utilize Ca^{2+} as a second messenger. Organelles of the secretory pathway often participate in both release and uptake of Ca^{2+}. One emerging concept is that the classical ER-Ca^{2+} store closely interacts with the endolysosomal compartment and other acidic organelles, thereby encoding complex cellular Ca^{2+} signals (14). It is thought that the IP_3R within the ER is important for Ca^{2+} refilling of lysosomes (15, 16). Recently, it was suggested that TPC1-dependent formation of ER–endosome contact sites mediates local Ca^{2+} signals (17, 48). Here, we propose a mechanism consistent with the concept that disturbed ER–endolysosomal interactions in TPC1-deficient mast cells abolish the exchange of Ca^{2+} between endolysosomes and the ER. Consequently, increased resting ER-Ca^{2+} concentrations, $[Ca^{2+}]_{ER}$, result in altered Ca^{2+} homeostasis, triggering enhanced histamine release (Fig. 4*F*). Accordingly, *Tpc1*$^{-/-}$ mast cells exhibited increased resting $[Ca^{2+}]_{ER}$, evaluated via Fura-2-FF and Mag-Fluo-4, but reduced endolysosomal $[Ca^{2+}]$ levels, visualized via GPN-induced rupture of lysosomes. Although the mechanism of action of GPN has been challenged recently (49), previous observations that perforation of lysosomal membranes (using GPN) increased IP_3-induced Ca^{2+} signals (39) support our concept. Moreover, our results argue against a direct action of GPN on the ER itself (49). It is likely that $PI(3,5)P_2$, a phosphoinositide (PIP) present in endolysosomal membranes, maintains the Ca^{2+} cross-talk via TPC1 activation, allowing for refill of endolysosomes by the ER via a Ca^{2+}–H^+ antiporter and/or direct contact sites and at the same time preventing ER-Ca^{2+} overload. If $PI(3,5)P_2$ activates TPC1 in the endolysosomal membrane, it will boost Ca^{2+} release via IP_3R (17, 48), and, locally, Ca^{2+}–H^+ antiporter will immediately buffer Ca^{2+} into the endolysosomal compartment. However, a TPC1-mediated Ca^{2+} release itself might not be sufficient to induce degranulation unaided in murine mast cells. This notion is supported by our findings that intracellular administration of $PI(3,5)P_2$ or NAADP via the patch pipette did not increase cell capacitance in electrophysiological whole-cell recordings of Tpc1$^{+/+}$ mast cells. However, simultaneous activation of TPC channels via application of $PI(3,5)P_2$ resulted in reduced GTPγS-induced degranulation responses in mast cells, reflected in diminished degranulation amplitudes and slower kinetics, while it displayed no effect on *Tpc1*$^{-/-}$ mast cell degranulation. The effect of simultaneous NAADP application together with GTPγS was less

severe but supports the same notion. The very recent identification of two structurally distinct TPC2 agonists, mirroring NAADP and PI(3,5)P_2 activation characteristics, suggests diverse ion channel selectivity depending on the mode of activation (50). However, whether TPC1 also switches its ion selectivity remains to be established, and TPC2 does not seem to be involved in degranulation of preformed mast cell granules. We conclude that TPC1 activation prevents Ca^{2+} overload of ER stores, thus warranting regulated degranulation. Consequently, we propose a model (Fig. 4*F*) stating that, in TPC1-deficient mast cells, more Ca^{2+} is released from the ER upon IgE/$F_c\varepsilon$R stimulation, while less is taken up into acidic granules, because TPC1-mediated contact between these organelles is lacking, thereby further augmenting exocytic processes and histamine release in mast cells. We propose that the interaction between the ER and the endolysosomal compartment is essential to prevent $[Ca^{2+}]_{ER}$ overload and subsequent overreactivity of immune cells. Accordingly, TPC1 is a critical component responsible for the endolysosomal Ca^{2+}-buffering capacity, thereby controlling the filling of the largest Ca^{2+} store, the ER, cytosolic Ca^{2+} signals, and exocytosis of mast cells ex vivo and in vivo.

The worldwide prevalence of allergic and anaphylactic reactions has increased tremendously over the last decades, and mast cells are essential drivers of these diseases (1, 2). Here, we link TPC1 deletion to enhanced passive systemic anaphylaxis in an in vivo animal model. Interestingly, we observed a significantly augmented drop in the body temperature in *Tpc1*$^{-/-}$ mice, which was also reflected in a slower recovery compared to wild-type animals. We assume that the drop in body temperature can be directly linked to enhanced vasodilatation due to more histamine released from TPC1-deficient mast cells and basophils. Ex vivo pharmacologic activation of TPCs slowed the degranulation rate and the Ca^{2+} release. Thus, our study highlights TPC1 channels as pharmacological targets for the treatment of mast cell-related diseases, such as allergies and anaphylaxis. Translational studies will now be necessary to confirm similar mechanisms in humans.

Materials and Methods

Mice and In Vitro Experiments. Mice were bred and raised in individually ventilated cages (Tecniplast) in the animal facility of the Walther-Straub-Institute at the Ludwig-Maximilians-University of Munich, according to the guidelines of the Federation for Laboratory Animal Science Associations. Mice were kept at a constant temperature of 20 °C, with a 12-h on/off light cycle, and with water and food ad libitum.

The *Tpc1*$^{-/-}$ mouse strain was generated through targeted deletion of Exon 3 of the *TPCN1* gene using the Cre-loxP recombination system (27, 31). Briefly, we generated, first, a mouse line containing a "floxed" exon 3 TPC1 allele. These mice were crossed with ROSA26 Cre mice to obtain a global TPC1 knockout line. Sequence analysis revealed a deletion of exon 3 and a frameshift and premature stop codon in the TPC1 complementary DNA. The utilized homozygous TPC1-deficient mice were back-crossed for 12 generations with C57BL/6NJ mice (Janvier Labs). Genotype identification of all herein deployed mice including age-matching wild-type animals with the same genetic background used as controls was performed by allele-specific PCR analysis as described previously (31). The *Tpc2*$^{-/-}$ mouse strain was generated as described previously (26).

Passive Systemic Anaphylaxis. For anaphylaxis experiments, littermate *Tpc1*$^{-/-}$ and Tpc1$^{+/+}$ offspring from *Tpc1*$^{+/-}$ intercrosses were used. All animal procedures fulfilled the German authorization guidelines for care and use of laboratory animals (officially approved by the Karlsruhe regional council). For the measurements of body temperature, we implanted temperature transponders (IPT 300, Bio Medic Data Systems) subcutaneously under Isoflurane anesthesia (51). Two days after the implantation procedure, the mice were sensitized by i.v. injection of anti-DNP IgE antibody (Sigma-Aldrich; final concentration 120 μg/kg of body weight) under Isoflurane anesthesia. Systemic anaphylactic reaction was elicited 24 h after mice sensitization by i.v. application of antigen solution under Isoflurane anesthesia. To this end, mice were injected with DNP-BSA (Sigma-Aldrich) at a dose of 2.7 mg/kg of body weight. Body temperature changes were measured every 5 min over a period of 2 h.

Primary Cell Culture and Cell Lines. Cell isolation from the peritoneum was done as described previously (34). Briefly, after cervical dislocation, the peritoneum of the mouse was flushed with cold Hanks balanced salt solution (HBSS). Harvested cells were subsequently centrifuged at 170 relative centrifugal force (rcf), 4 °C, for 10 min, and the supernatant was discarded. Cells were either directly processed for electron microscopy or Western blot analysis, or resuspended in Dulbecco's modified Eagle medium (DMEM), supplemented with 10% fetal bovine serum (FBS) (PAA) and 1% Penicillin/Streptomycin (Thermo Fisher Scientific). After seeding the cells on poly-L-lysine-coated glass coverslips (Sigma-Aldrich), cells were recovered overnight in a humidified incubator (37 °C, 5% CO_2) before they were used for Ca^{2+} imaging experiments, patch clamp studies, or different staining procedures.

For enrichment and culture of PMCs, PMCs were isolated by intraperitoneal (i.p.) lavage and cultured 14 d to 16 d in RPMI Medium supplemented with 20% FBS [1% Penicillin/Streptomycin, 10 ng/mL IL-3 and 30 ng/mL SCF at the concentration 1×10^6 cells/mL in 5% CO_2 at 37 °C as described before (33)]. After the i.p. lavage, suspension of the cells isolated from three mice were pooled and cultured together as one preparation.

Bone marrow cells were isolated from wild-type and TPC1-deficient animals by flushing femurs with ice-cold HBSS using a 1-mL syringe attached to a 23-gauge needle (52). After three washings with ice-cold HBSS (1,500 rpm, 7 min), harvested cells were resuspended in lysis buffer and stored for 30 min on ice before being examined by Western blot analysis.

The rat basophilic leukemia cell line, RBL-1, was cultured in DMEM supplemented with 10% FBS (Gibco, Thermo Fisher Scientific), 1× MEM Non-Essential Amino Acids Solution (Gibco, Thermo Fisher Scientific), and 1 mM Sodium Pyruvate (Thermo Fisher Scientific).

Western Blot Analysis. Isolated peritoneal cells, bone marrow cells and CD117$^+$ cells, resuspended in ice-cold lysis buffer (10 mM Tris/HCl pH 8, 5% glycerol, 1 mM (ethylenedinitrilo)tetraacetic acid [EDTA], 67.5 mM NaCl, 0.5% Triton X-100, 0.1 mg/mL DNase, complete protease inhibitor EDTA-free [Roche]), were incubated for 30 min on ice; subsequent lysate, separated by centrifugation (10 min, 12500 rcf), was transferred to a new reaction tube and mixed with 4× Laemmli sample buffer.

Equal volumes of cell lysates from wild-type or *Tpc1*$^{-/-}$ animals were separated by sodium dodecyl sulfate polyacrylamide gel electrophoresis (10%) and transferred to nitrocellulose membranes using a semidry blotting system; equal protein loading and immobilization of samples of both genotypes was confirmed by Ponceau S staining.

After removing red staining by washing nitrocellulose sheets with double-distilled water, nonspecific binding sites on the nitrocellulose membranes were blocked with 5% powdered nonfat milk in 10 mM Tris/HCl, pH 8.0, 150 mM NaCl, and 0.05% Tween 20 (TBST); blots were incubated overnight at 4 °C with a specific rabbit anti-TPC1 antibody (31, 32), diluted in TBST, and supplemented with 3% powdered milk; an antibody recognizing β-actin (Sigma-Aldrich, catalog no: A2066) served as additional loading control. After three washing steps with TBST, membranes were incubated with a horseradish peroxidase-conjugated anti-rabbit secondary antibody (Bio-Rad), diluted in 3% milk powder/TBST. After incubation for 1 h at room temperature (RT), membranes were washed three times with TBST to remove unbound antibodies. Binding of primary antibodies was then visualized using the enhanced chemiluminescence system and an automated chemiluminescence system (Chemismart, Peqlab). The observed broad immunoreactive band can be explained by diverse glycosylation patterns of TPCs (53).

TEM and Morphological Analysis of Mast Cells. Preparation of mast cell samples for ultrastructural examination by TEM was performed as described previously (54). Briefly, isolated peritoneal cells of wild-type and TPC1-deficient animals were resuspended in phosphate buffer (100 mM PO_4, pH 7.2) containing 2.5% glutaraldehyde, and then fixed for 4 h at RT. Fixed cells were subsequently collected, rinsed several times in phosphate buffer only (10 min at 200 rcf), and then postfixed in 1% osmium tetroxide (in H_2O) for 1.5 h at 4 °C. Afterward, samples were dehydrated in an ascending acetone series and embedded in epoxy embedding medium (Sigma-Aldrich). Ultrathin sections contrasted with methylene blue were examined using a Zeiss transmission electron microscope (EM902A). Morphological analyses were performed for 21 wild-type and TPC1-deficient mast cells (four individuals per genotype) using the Image J software (https://imagej.net/Welcome).

Cell Surface Staining for Flow Cytometric Analysis. Labeling of cell-type specific surface antigens of cells isolated from the peritoneal cavity was performed as described recently (54). Briefly, after saturating unspecific binding sites with mouse F_cR-blocking reagent (Miltenyi Biotech) (10% blocking solution in 0.5% BSA, 2 mM EDTA in PBS [magnetic-activated cell sorting [MACS] buffer]) for 10 min at 4 °C, cells were harvested by centrifugation (1,500 rpm, 5 min, 4 °C) and subsequently resuspended in MACS buffer, also used to dilute immune-phenotyping antibodies (T cells: CD3; B cells: B220; macrophages: CD11b, mast cells: CD117; neutrophils: Ly6-G), (working dilution 1:100, each). After an incubation of 20 min at RT, excess antibodies were eliminated by three washing steps with MACS buffer (1,500 rpm, 5 min, 4 °C). Flow cytometric analysis was performed with a Guava easy Cyte single sample flow cytometer (Merck-Millipore); isotype controls were used as references. Gates were adjusted on live cells and cell size. Resulting populations were analyzed for fluorescence signals. Data were analyzed using the InCyte software (Merck-Millipore). Sorting of $CD117^+$ cells was performed with fluorescence-activated cell sorter Aria.

Histamine Assay. Histamine release was quantified using a competitive immunoassay according to the manufacturer's instructions (Homogeneous Time Resolved Fluorescence histamine assay, catalog no. 62HTMPEB, Cisbio Bioassays).

In brief, mast cells isolated by peritoneal lavage were incubated in an external solution containing 140 mM NaCl, 1 mM $CaCl_2$, 2.8 mM KCl, 2 mM $MgCl_2$, 10 mM Hepes/NaOH, and 11 mM glucose (pH 7.2, 300 mOsmol·L^{-1}) for 30 min at RT. For mast cell stimulation, the synthetic secretagogue compound 48/80 (30 μg/mL) (Sigma-Aldrich) or the Ca^{2+} ATPase inhibitor TG (2 μM) was added to the solution (30 min, RT). To determine the entire histamine content, freshly isolated cells from the lavage were lysed with 0.5% Triton X-100. Histamine levels were determined from peritoneal lavage obtained from at least three animals of each genotype, with triplicate determinations.

β-Hexosaminidase Assay. Cells were resuspended at concentration 2×10^6 cells per mL in Tyrode solution containing (millimolars): NaCl 130; KCl 5; $CaCl_2$ 1.4; $MgCl_2$ 1; glucose 5,6; Hepes 10, 0, 1% BSA (Fraction V); pH 7.4 adjusted with NaOH. Some cells were resuspended in the Tyrode solution with adding of 500 nM *Tet*. The PMCs (100 μL per well) were seeded in a V-bottom 96-well plate (Corning Costar; COS3896) and incubated 15 min at 37 °C. Thereafter, 25 μL of solution supplemented with corresponding agonists/antagonists was added. The cells were incubated for 45 min at 37 °C. After a short centrifugation step (1,000 × *g* for 5 min at 4 °C), the supernatants and the cell pellets were separated. The cell pellets were lysed for 5 min at RT with the Tyrode solution containing 1% Triton-X. Lysates and supernatants were incubated separately with 2 mM of the colorigenic substrate 4-nitrophenyl *N*-acetyl-β-D-glucosaminide (Sigma-Aldrich) for 1 h at 37 °C. The reaction was stopped by adding of 150 μL of 200 mM glycine (pH 10.7 with NaOH) to 50 μL of the reaction mixture. The absorbance (at 405 nm) of the resulting probes was quantified using a NanoQuant infinite M200pro (Tecan) spectrophotometer. The percentage of β-hexosaminidase release was calculated as a ratio of absorbance of the supernatant to the total (sum of supernatant and lysate) β-hexosaminidase content.

Ca^{2+} Imaging.

Fura-2/Fura-2FF measurements. Ca^{2+} mobilization of cells was performed using a single-cell imaging system of TillPhotonics and the Fura-2–based ratiometric spectrometry. After isolation, peritoneal cells were seeded on poly-L-lysine coated coverslips (20,000 cells per cm^2) and incubated overnight to recover. For IgE/DNP-BSA stimulation experiments, incubation buffer (DMEM, 10% FBS, 1% Penicillin/Strepomycin) was additionally supplemented with IgE (100 ng/mL; Sigma-Aldrich). Cells were then loaded with Fura-2 AM (5 μM) (Sigma-Aldrich) for 30 min at 37 °C in a Na^+ Ringer solution (140 mM NaCl, 1 mM $CaCl_2$, 2,8 mM KCl, 2 mM $MgCl_2$, 10 mM Hepes NaOH, 11 mM glucose), containing 1% BSA and 0.02% Pluronic acid (Sigma-Aldrich, pH 7.2). For experiments with the low-affinity Ca^{2+} fluorochrome Fura-2FF AM (Biomol) (41), cells were loaded for 45 min using the same supplemented Na^+ Ringer. Unbound dye was eliminated by two washings. For recordings under Ca^{2+}-free conditions, cells were transferred to a Ca^{2+}-free Na^+ Ringer solution where $CaCl_2$ was replaced by 0.5 mM ethylene glycol-bis(2-aminoethyl ether)-N,N,N′,N′-tetraacetic acid (EGTA). Mast cells were identified visually under the light microscope (phase contrast), and regions of interest (ROIs) were set using the TILLvision software 4.0. After establishing a baseline, respective substances were added (DNP-BSA, Sigma-Aldrich; TG, Sigma-Aldrich; GPN, Santa Cruz-Biotechnology; *Tet*, Sigma-Aldrich; *trans*-Ned-19, Tocris), as indicated for each experiment. To assess dye loading and cell viability, experiments were always finished by treating the cells with either 2 μM TG or the addition of Ringer solution supplemented with 2 mM $CaCl_2$. Fura-2 ratios (F_{340nm}/F_{380nm}) were calculated as quotient of the detected fluorescence intensities at 510 nm after emission in response to 340/380 nm excitation.

Mast cell Mag-Fluo-4 measurements. Ca^{2+} mobilization of mast cells was performed using a single-cell imaging system of Zeiss with a Colibri-2 LED-Illumination System. Peritoneal cells were isolated, seeded on coverslips, and incubated overnight as previously described for the Fura-2/Fura-2FF measurements. The dye loading was performed at RT for 40 min, using 3.7 μM Mag-Fluo-4 AM (Sigma-Aldrich) in Na^+ Ringer solution. Cells were then washed with and transferred into Ca^{2+}-free Na^+ Ringer solution, containing 0.5 mM EGTA. The washing was followed by 5 min of permeabilization with digitonin (16 μM) in intracellular solution (ICS) containing (in millimolars): 125 KCl, 25 NaCl, 10 Hepes, 0.5 MgATP, 0.5 $MgCl_2$, 0.2 $CaCl_2$, and 0.5 EGTA, pH 7.25, supplemented with an ATP regenerating system consisting of 10 μg/mL creatine phosphokinase Type I and 10 mM phosphocreatine (42). The permeabilization was stopped by two washings with digitonin-free ICS. Mast cells were then identified visually under the light microscope, and ROIs were set. The emission was measured at 517 nm, after excitation at 493 nm, and images were analyzed via the ZEN Software. After establishing a baseline, the mast cells were stimulated with IP_3 (5 μM).

RBL-1 cell Mag-Fluo-4 measurements. Ca^{2+} mobilization of RBL-1 was performed using a single-cell imaging system of Zeiss with a Colibri-2 LED-Illumination System. RBL-1 cells were seeded on poly-L-lysine coated coverslips (40,000 cells per cm^2) and incubated overnight. They were loaded with Mag-Fluo-4 AM (5 μM) (Sigma-Aldrich) for 40 min at RT in a Na^+ Ringer solution. Cells were then washed with and transferred into Ca^{2+}-free Na^+ Ringer solution, containing 0.5 mM EGTA and treated with or without *Tet* (500 nM) for 15 min. Cells were then again identified visually under the light microscope, ROIs were set, and images were analyzed via the ZEN Software. Then, the measuring chamber was initially perfused with digitonin (20 μM) for 8 s in ICS. After washing with ICS and establishing a baseline, IP_3 (5 μM) was perfused (55).

ER-Tagged Aequorine Ca^{2+} Measurements. Transfections were carried out using the Cell Line Nucleofector Kit V (Lonza). The pcDNA3.1+/ER-2mutAEQ was a gift from Javier Alvarez-Martin (Addgene plasmid #45541). After electroporation, ~4×10^6 cells were seeded on one cavity of a six-well dish. After 24 h, culture medium was replaced with external solution containing (in micromolars): NaCl, 145; KCl, 5; $MgCl_2$, 1; glucose, 10; Hepes, 10, pH 7.4, supplemented with 0.5 mM EGTA with or without 500 nM *Tet* (56). After 15 min at RT, cells were challenged with 20 μM CPA for an additional 15 min. After CPA was removed, cells were incubated with 5 μM coelenterazine i for 90 min at RT. Within this time period, *Tet* was also added to the treated cells. Cells were then mechanically removed and seeded on six cavities (for each condition) of white 96-well plates. Total light emission was detected in a BMG PolarStar for 0.3 s every 0.3 s for a total of 150 s. After 20 s, $CaCl_2$ (2.5 mM final) were automatically injected.

Electrophysiology. Degranulation of wild-type and TPC1/2-deficient PMCs was analyzed by measuring cell membrane capacitance using the patch clamp technique as previously described (34). In brief, using the automated capacitance cancellation function of the EPC-9/10 (HEKA), measurements were done in a tight seal whole-cell configuration at RT. Current voltage dependencies were monitored in voltage clamp experiments (holding potential of 0 mV at 0.5 Hz), applying a ramp protocol of −100 mV to +100 mV over 50 ms. Membrane capacitance values directly captured after breaking a seal between the membrane and the glass pipette were used as a reference for the initial cell surface area. Further recorded values were normalized to this initial determined capacitance. The external solution consisted of 140 mM NaCl, 1 mM $CaCl_2$, 2.8 mM KCl, 2 mM $MgCl_2$, 10 mM Hepes/NaOH, 11 mM glucose (pH 7.2, 300 mOsmol·L^{-1}); the internal solution was composed of 120 mM potassium glutamate, 8 mM NaCl, 1 mM $MgCl_2$, 10 mM Hepes (pH 7.2, 280 mOsmol·L^{-1}). For stimulation of cells, either the non-hydrolyzable GTP analog GTPγS (100 μM) (Sigma-Aldrich) or GTPγS (100 μM) was used alone or in conjunction with NAADP (1 μM) or $PI(3,5)P_2$ (10 μM) (Mobitec), and applied directly through the patch pipette; the TPC inhibitor *Tet* (500 nM) was added to the external solution. Values for maximum degranulation amplitudes were taken 300 s after stimuli application. Kinetic parameters of the degranulation reaction, such as the onset time point of secretion (delay) or the rate of degranulation (tau) were determined by fitting obtained data with a capacitance fit, using the IgorPro software (34). The following fit function was applied: $f(x) = c_{initial} + (c_{initial} \times (c_{max} - 1) \times (1 - \exp(-(t_{delay})/\tau))^n)$.

Statistics. Data are presented as mean values ±SEM unless otherwise indicated in the figure legends. Statistical analysis was done via Excel 2010 or the Graphpad Prism software (version, 7.0). Significant differences between groups were analyzed using an unpaired Student's *t* test or ANOVA with Tukey's multiple comparison post hoc test; levels of statistical significance (*P* values) are indicated by asterisks (*: $P < 0.05$; **: $P < 0.01$; ***: $P < 0.001$).

Data Availability. The data are made available in the paper.

ACKNOWLEDGMENTS. We thank Sheila Geiger, Renate Heilmair, Dorothea Schünke, Holger Jastrow, and Lisa Fahr for technical assistance, and Hermann Kalwa for scientific advice. We thank the following funding agencies: M.F., T.G., I.B., and S.Z. were supported by the Deutsche Forschungsgemeinschaft (DFG, German Research Foundation) (Grant BO 1665/5-2 and Project 239283807 as well as TRR-152/2 Projects 14 [S.Z.], 15 [T.G.], and 21 [M. Freichel]), and by the DFG Priority Program 1394: "Mast Cells—Promoters of Health and Modulators of Disease," FOR 2289, the German Centre for Cardiovascular Research, and the German Ministry of Education and Research (M. Freichel).

1. P. Poowuttikul, D. Seth, Anaphylaxis in children and adolescents. *Pediatr. Clin. North Am.* **66**, 995–1005 (2019).
2. J. E. Yu, R. Y. Lin, The epidemiology of anaphylaxis. *Clin. Rev. Allergy Immunol.* **54**, 366–374 (2018).
3. D. D. Metcalfe *et al*., Biomarkers of the involvement of mast cells, basophils and eosinophils in asthma and allergic diseases. *World Allergy Organ. J.* **9**, 7 (2016).
4. D. P. Evans, D. S. Thomson, Histamine release from rat mast cells passively sensitised with homocytotropic (IgE) antibody. *Int. Arch. Allergy Appl. Immunol.* **43**, 217–231 (1972).
5. K. A. Lindstedt, P. T. Kovanen, Isolation of mast cell granules. *Curr. Protoc. Cell Biol.* **29**, 3.16.1–3.16.13 (2006).
6. S. Bulfone-Paus, G. Nilsson, P. Draber, U. Blank, F. Levi-Schaffer, Positive and negative signals in mast cell activation. *Trends Immunol.* **38**, 657–667 (2017).
7. F. Siebenhaar, F. A. Redegeld, S. C. Bischoff, B. F. Gibbs, M. Maurer, Mast cells as drivers of disease and therapeutic targets. *Trends Immunol.* **39**, 151–162 (2018).
8. Y. C. Chen *et al*., Differential Ca^{2+} mobilization and mast cell degranulation by FcεRI- and GPCR-mediated signaling. *Cell Calcium* **67**, 31–39 (2017).
9. N. Gaudenzio *et al*., Different activation signals induce distinct mast cell degranulation strategies. *J. Clin. Invest.* **126**, 3981–3998 (2016).
10. R. Vennekens *et al*., Increased IgE-dependent mast cell activation and anaphylactic responses in mice lacking the calcium-activated nonselective cation channel TRPM4. *Nat. Immunol.* **8**, 312–320 (2007).
11. Y. Baba *et al*., Essential function for the calcium sensor STIM1 in mast cell activation and anaphylactic responses. *Nat. Immunol.* **9**, 81–88 (2008).
12. M. Vig *et al*., Defective mast cell effector functions in mice lacking the CRACM1 pore subunit of store-operated calcium release-activated calcium channels. *Nat. Immunol.* **9**, 89–96 (2008).
13. H. T. Ma, M. A. Beaven, Regulation of Ca^{2+} signaling with particular focus on mast cells. *Crit. Rev. Immunol.* **29**, 155–186 (2009).
14. S. Patel, R. Docampo, Acidic calcium stores open for business: Expanding the potential for intracellular Ca^{2+} signaling. *Trends Cell Biol.* **20**, 277–286 (2010).
15. A. G. Garrity *et al*., The endoplasmic reticulum, not the pH gradient, drives calcium refilling of lysosomes. *eLife* **5**, e15887 (2016).
16. P. Atakpa, N. B. Thillaiappan, S. Mataragka, D. L. Prole, C. W. Taylor, IP3 receptors preferentially associate with ER-lysosome contact sites and selectively deliver Ca^{2+} to lysosomes. *Cell Rep.* **25**, 3180–3193.e7 (2018).
17. B. S. Kilpatrick, E. R. Eden, A. H. Schapira, C. E. Futter, S. Patel, Direct mobilisation of lysosomal Ca^{2+} triggers complex Ca2+ signals. *J. Cell Sci.* **126**, 60–66 (2013).
18. B. S. Kilpatrick *et al*., An endosomal NAADP-sensitive two-pore Ca^{2+} channel regulates ER-endosome membrane contact sites to control growth factor signaling. *Cell Rep.* **18**, 1636–1645 (2017).
19. E. Brailoiu *et al*., Essential requirement for two-pore channel 1 in NAADP-mediated calcium signaling. *J. Cell Biol.* **186**, 201–209 (2009).
20. P. J. Calcraft *et al*., NAADP mobilizes calcium from acidic organelles through two-pore channels. *Nature* **459**, 596–600 (2009).
21. M. Ruas *et al*., Purified TPC isoforms form NAADP receptors with distinct roles for Ca^{2+} signaling and endolysosomal trafficking. *Curr. Biol.* **20**, 703–709 (2010).
22. A. J. Morgan, L. C. Davis, M. Ruas, A. Galione, TPC: The NAADP discovery channel? *Biochem. Soc. Trans.* **43**, 384–389 (2015).
23. X. Wang *et al*., TPC proteins are phosphoinositide- activated sodium-selective ion channels in endosomes and lysosomes. *Cell* **151**, 372–383 (2012).
24. J. She *et al*., Structural insights into the voltage and phospholipid activation of the mammalian TPC1 channel. *Nature* **556**, 130–134 (2018).
25. C. Grimm, C. C. Chen, C. Wahl-Schott, M. Biel, Two-pore channels: Catalyzers of endolysosomal transport and function. *Front. Pharmacol.* **8**, 45 (2017).
26. C. Grimm *et al*., High susceptibility to fatty liver disease in two-pore channel 2-deficient mice. *Nat. Commun.* **5**, 4699 (2014).
27. Y. Sakurai *et al*., Ebola virus. Two-pore channels control Ebola virus host cell entry and are drug targets for disease treatment. *Science* **347**, 995–998 (2015).
28. L. C. Davis *et al*., NAADP activates two-pore channels on T cell cytolytic granules to stimulate exocytosis and killing. *Curr. Biol.* **22**, 2331–2337 (2012).
29. J. P. Luzio, Y. Hackmann, N. M. Dieckmann, G. M. Griffiths, The biogenesis of lysosomes and lysosome-related organelles. *Cold Spring Harb. Perspect. Biol.* **6**, a016840 (2014).
30. C. Grimm, E. Butz, C. C. Chen, C. Wahl-Schott, M. Biel, From mucolipidosis type IV to Ebola: TRPML and two-pore channels at the crossroads of endo-lysosomal trafficking and disease. *Cell Calcium* **67**, 148–155 (2017).
31. L. Arndt *et al*., NAADP and the two-pore channel protein 1 participate in the acrosome reaction in mammalian spermatozoa. *Mol. Biol. Cell* **25**, 948–964 (2014).
32. J. Castonguay *et al*., The two-pore channel TPC1 is required for efficient protein processing through early and recycling endosomes. *Sci. Rep.* **7**, 10038 (2017).
33. V. Tsvilovskyy *et al*., Deletion of Orai2 augments endogenous CRAC currents and degranulation in mast cells leading to enhanced anaphylaxis. *Cell Calcium* **71**, 24–33 (2018).
34. S. Zierler *et al*., TRPM7 kinase activity regulates murine mast cell degranulation. *J. Physiol.* **594**, 2957–2970 (2016).
35. T. C. Moon, A. D. Befus, M. Kulka, Mast cell mediators: Their differential release and the secretory pathways involved. *Front. Immunol.* **5**, 569 (2014).
36. N. Fukuishi *et al*., Does β-hexosaminidase function only as a degranulation indicator in mast cells? The primary role of β-hexosaminidase in mast cell granules. *J. Immunol.* **193**, 1886–1894 (2014).
37. B. Rituper *et al*., High-resolution membrane capacitance measurements for the study of exocytosis and endocytosis. *Nat. Protoc.* **8**, 1169–1183 (2013).
38. E. Naylor *et al*., Identification of a chemical probe for NAADP by virtual screening. *Nat. Chem. Biol.* **5**, 220–226 (2009).
39. C. I. López-Sanjurjo, S. C. Tovey, D. L. Prole, C. W. Taylor, Lysosomes shape Ins(1,4,5)P3-evoked Ca^{2+} signals by selectively sequestering Ca^{2+} released from the endoplasmic reticulum. *J. Cell Sci.* **126**, 289–300 (2013).
40. R. B. Lomax, C. Camello, F. Van Coppenolle, O. H. Petersen, A. V. Tepikin, Basal and physiological Ca^{2+} leak from the endoplasmic reticulum of pancreatic acinar cells. Second messenger-activated channels and translocons. *J. Biol. Chem.* **277**, 26479–26485 (2002).
41. V. A. Golovina, M. P. Blaustein, Spatially and functionally distinct Ca^{2+} stores in sarcoplasmic and endoplasmic reticulum. *Science* **275**, 1643–1648 (1997).
42. R. Chen *et al*., Bcl-2 functionally interacts with inositol 1,4,5-trisphosphate receptors to regulate calcium release from the ER in response to inositol 1,4,5-trisphosphate. *J. Cell Biol.* **166**, 193–203 (2004).
43. S. de la Fuente, R. I. Fonteriz, P. J. de la Cruz, M. Montero, J. Alvarez, Mitochondrial free [Ca^{2+}] dynamics measured with a novel low-Ca^{2+} affinity aequorin probe. *Biochem. J.* **445**, 371–376 (2012).
44. S. de la Fuente, R. I. Fonteriz, M. Montero, J. Alvarez, Ca^{2+} homeostasis in the endoplasmic reticulum measured with a new low-Ca^{2+}-affinity targeted aequorin. *Cell Calcium* **54**, 37–45 (2013).
45. W. Dammermann, A. H. Guse, Functional ryanodine receptor expression is required for NAADP-mediated local Ca^{2+} signaling in T-lymphocytes. *J. Biol. Chem.* **280**, 21394–21399 (2005).
46. S. Wernersson, G. Pejler, Mast cell secretory granules: Armed for battle. *Nat. Rev. Immunol.* **14**, 478–494 (2014).
47. H. Xu, N. R. Bin, S. Sugita, Diverse exocytic pathways for mast cell mediators. *Biochem. Soc. Trans.* **46**, 235–247 (2018).
48. M. J. Phillips, G. K. Voeltz, Structure and function of ER membrane contact sites with other organelles. *Nat. Rev. Mol. Cell Biol.* **17**, 69–82 (2016).
49. P. Atakpa, L. M. van Marrewijk, M. Apta-Smith, S. Chakraborty, C. W. Taylor, GPN does not release lysosomal Ca^{2+} but evokes Ca^{2+} release from the ER by increasing the cytosolic pH independently of cathepsin C. *J. Cell Sci.* **132**, jcs223883 (2019).
50. S. Gerndt *et al*., Agonist-mediated switching of ion selectivity in TPC2 differentially promotes lysosomal function. *eLife* **9**, e54712 (2020).
51. V. Tsvilovskyy, A. Solis-Lopez, K. Öhlenschläger, M. Freichel, Isolation of peritoneum-derived mast cells and their functional characterization with Ca^{2+}-imaging and degranulation assays. *J. Vis. Exp.* **137**, E57222 (2018).
52. X. Liu, N. Quan, Immune cell isolation from mouse femur bone marrow. *Bio Protoc.* **5**, e1631 (2015).
53. X. Zong *et al*., The two-pore channel TPCN2 mediates NAADP-dependent Ca^{2+}-release from lysosomal stores. *Pflugers Arch.* **458**, 891–899 (2009).
54. A. Romagnani *et al*., TRPM7 kinase activity is essential for T cell colonization and alloreactivity in the gut. *Nat. Commun.* **8**, 1917 (2017).
55. A. M. Hofer, C. Fasolato, T. Pozzan, Capacitative Ca^{2+} entry is closely linked to the filling state of internal Ca^{2+} stores: A study using simultaneous measurements of ICRAC and intraluminal [Ca^{2+}]. *J. Cell Biol.* **140**, 325–334 (1998).
56. J. Alvarez, M. Montero, Measuring [Ca^{2+}] in the endoplasmic reticulum with aequorin. *Cell Calcium* **32**, 251–260 (2002).